FULL PAPER

Large-Area, Periodic, Hexagonal Wrinkles on Nanocrystalline Graphitic Film

Yanpeng Liu, Kenry, Yufeng Guo, Surabhi Sonam, Seul Ki Hong, Mui Hoon Nai, Chang Tai Nai, Libo Gao, Jianyi Chen, Byung Jin Cho, Chwee Teck Lim, Wanlin Guo, and Kian Ping Loh**

Sinusoidal wrinkles develop in compressively stressed film as a means to release stored elastic energy. Here, a simple way to fabricate large-area, periodic, hexagonal wrinkled pattern on nanocrystalline graphitic films grown on *c*-plane sapphire (<50 nm thick) by the spontaneous delamination–buckling of the as-grown film during cooling is reported. According to the continuum mechanics calculation, strain-relief pattern adopting the hexagonal wrinkled pattern has a lower elastic energy than that of the telephone cord wrinkle at thickness regime below 50 nm. A high-fidelity transfer method is developed to transfer the hexagonal wrinkled films onto arbitrary substrates. Nanoindentation studies show that hexagonal wrinkle film engineered this way may act as shock absorber. The hexagonal wrinkled carbon film is able to selectively promote the differentiation of human mesenchymal stem cell toward the osteogenic lineage in the absence of osteogenic inducing medium.

Y. Liu, Dr. L. Gao, Dr. J. Chen, Prof. K. P. Loh
Department of Chemistry
and Graphene Research Center
National University of Singapore
3 Science Drive 3, Singapore 117543, Singapore
E-mail: chmlohkp@nus.edu.sg
Y. Liu
NanoCore
National University of Singapore
Singapore 117576, Singapore
Kenry, Dr. S. Sonam, Prof. C. T. Lim
Department of Biomedical Engineering
National University of Singapore
9 Engineering Drive 1, Singapore 117575, Singapore
Kenry, C. T. Nai, Prof. C. T. Lim
NUS Graduate School for Integrative Sciences and Engineering
28 Medical Drive #05-01, Singapore 117597, Singapore
Prof. Y. Guo, Prof. W. Guo
State Key Laboratory of Mechanics and Control of Mechanical Structures
Key Laboratory for Intelligent Nano Materials
and Devices of Ministry of Education and Institute of Nano Science
Nanjing University of Aeronautics and Astronautics
Nanjing 210016, China
E-mail: wlguo@nuaa.edu.cn
S. K. Hong, Prof. B. J. Cho
Department of Electrical Engineering
KAIST, 291 Daehak-Ro, Yuseong-gu, Daejeon 305-701, South Korea
Dr. M. H. Nai, Prof. C. T. Lim
Mechanobiology Institute
National University of Singapore
7 Engineering Drive 1, Singapore 117574, Singapore

DOI: 10.1002/adfm.201502010

1. Introduction

Surface wrinkles develop on compressively strained films due to elastic stress relaxation. These wrinkles can self-organize to form undulating patterns on surfaces. The origin of special geometrical shapes adopted by the wrinkles are not well understood, as it arises from a complex interplay of buckling and delamination forces, as well as horizontal relaxation on the nonbuckled domains. Nonetheless, if such periodic wrinkles can be generated over large area, they can be potentially used as shock absorbers due to its large elastic moduli, and even as cell-culture template due to its biomimetic topography. Strain engineering of various sorts has been applied to generate periodic wrinkles on thin films,[1–5] these include sequential release of biaxially stretched film on soft substrates,[6,7] focused ion beam irradiation of a polymeric substrate,[8] laser path-guided wrinkling,[9] solvent-responsive wrinkling,[10–12] or thermally mismatched contraction on polymer substrates.[13] However, all these methods are quite involved in terms of equipment and processes and not readily scalable. Although graphene can be deformed readily out of plane, only mesoscopic corrugation can be supported on it. To support micrometer high corrugation over a large area, the film has to be sufficiently thick to possess sufficient rigidity. In previous studies, the wrinkled films were intimately attached to the substrate imposing the strain, which means that it is not easy to transfer these wrinkled films onto another substrate, thus limiting their technological applications.[4,5,13,14]

Buckling–delamination of multilayered carbon films on rigid substrates can be a facile method to produce large-scale, periodically wrinkled film. Due to thermal expansion coefficient difference and high built-in stress, strain-relief features such as circular, straight-sided, telephone cord (or herringbone) and network wrinkles have been produced.[15–17] Spontaneous buckling occurs when the intrinsic stress of films surpasses critical compressive biaxial stress at the onset of buckling σ_c[15,18]

$$\sigma_c = \frac{\pi^2 E_f}{12\left(1-\nu_f^2\right)}\left(\frac{2t}{W}\right)^2 \quad (1)$$

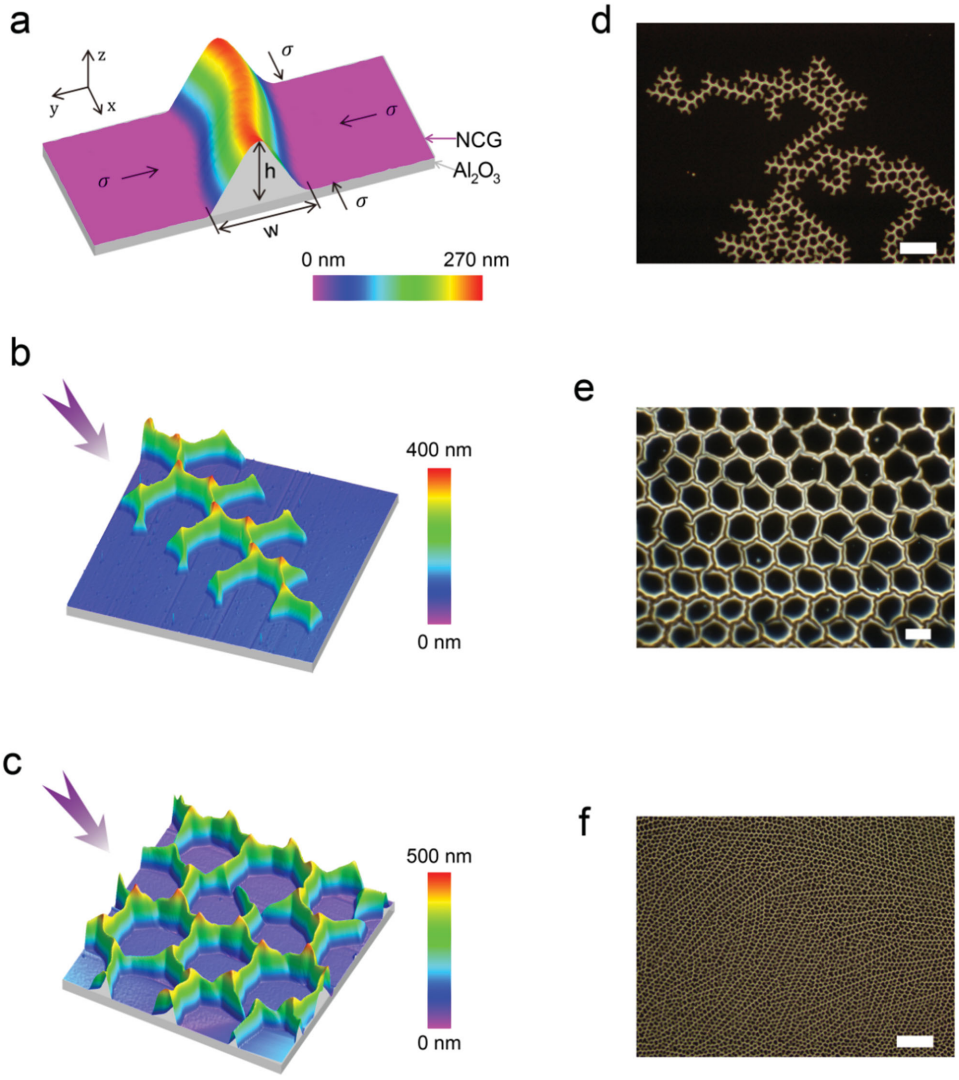

Figure 1. AFM and optical images of delaminated wrinkles of NCG films on sapphire substrates. a) Three dimensional(3D) AFM images of a typical buckling-delaminated thin NCG films at the non-node area. b) 3D AFM mapping of the propagation tip during the delamination process. For NCG films with a thickness of 24 nm, it takes up to 2 d to complete the delamination process for a 1 cm × 1 cm size sample. c) AFM topography of hexagonal wrinkles after the delamination process was adequate completed. d) Optical image of boundary region under dark field mode. e,f) Dark field images of hexagonal wrinkles under different magnifications. Scale bars in (d), (e), and (f) are 50, 10, and 100 μm, respectively.

where E_f is the Young's modulus, ν_f is the Poisson's ratio, t is the film thickness, and W is the full width of the wrinkle as indicated in **Figure 1**a.

For any given internal stress σ_0, the full width of delamination wrinkle, W_0 can be expressed as[18]

$$W_0 = \frac{\pi t}{\sqrt{3}}\sqrt{\frac{E_f}{(1-\nu_f^2)\sigma_0}} \tag{2}$$

From the above two equations, internal stress σ_0 and film thickness t affect the geometry of vertical wrinkles. In order to obtain repeated unit for propagation and large-scale high periodic wrinkled pattern, a uniform σ_0 and t is essential.

To propagate the pattern over large area, we need to consider the average energy release rate (R) of the delamination process. According to the Euler model[19–22]

$$R = \frac{(1-\nu_f^2)\sigma_0^2 t}{2E_f}(\sigma_0 - \sigma_c)(\sigma_0 + 3\sigma_c) \tag{3}$$

A steady-state energy release rate is needed for the uniform spread of repeat units rather than a chaotic wrinkled pattern.

To predict the buckling pattern of thin films with small overstress (σ_0/σ_c slightly over 1), Hutchinson and co-workers[23] analyzed the expansion of normalized elastic energy U/U_0, and applied upper-bound analysis for four types of stress-relief patterns

$$\frac{U}{U_0} = 1 - Q\left(\frac{\sigma_0 - \sigma_c}{\sigma_c}\right)^2 + \cdots \tag{4}$$

here U_0 and U are the elastic energy per unit area in the unbuckled and buckled state, respectively. The stress-relief patterns include

the straight-sided wrinkled pattern, where $Q = \frac{1+\nu_f}{2}$; and square checkerboard pattern, where $Q = \frac{2}{3-\nu_f}$; and hexagonal and triangular pattern, where $Q = \frac{6}{11-5\nu_f}$. The widely observed telephone cord pattern can be considered as a bifurcation of square checkerboard pattern. Generally for $\nu_f > 0.2$, checkerboard pattern has the lowest energy in this overstress range. We note that hexagonal wrinkled patterns extending over a wide area on rigid substrates have not been reported.[23] Motivated thus, we want to study the different thickness regimes where these hexagonal strain-relief features can propagate, and to study the relationship between elastic energy release and film thickness.

Herein, chemical vapor deposition was used to grow nanocrystalline graphitic (NCG) films on *c*-plane sapphire substrates. At thickness below 50 nm, the NCG film formed periodic wrinkles with a hexagonal pattern upon cooling. These wrinkled films were uniform over a large area and could be transferred onto arbitrary substrates using an etch-free dry transfer process. Our studies show that wrinkled NCG promoted the differentiation of human mesenchymal stem cells (hMSCs) toward the osteogenic lineage in the absence of osteogenic inducing media. Compared to flat films, the wrinkled films exhibited increased reflectance loss in electromagnetic interference shielding and enhanced electrochemical performances (see Figures S14 and S15 in the Supporting Information).

2. Results

NCG film was grown on polished sapphire substrate (0001) by chemical vapor deposition using toluene as the carbon source. Uniform NCG films of various thicknesses were produced by controlling the growth time. The chemical phase of the NCG film was evaluated by Raman spectroscopy and XPS (X-ray photoelectron spectroscopy, see Figure S3 in the Supporting information), which revealed that it was a multilayered graphitic film. After cooling to room temperature, the buckling–delamination process occurred spontaneously on the as-deposited flat NCG films. The NCG films released the build-in stress by forming hexagonal wrinkles at a thickness-dependent speed (see Movie S1 in the Supporting Information). For NCG films with thickness ranging from 24 ± 2 to 35 ± 3 nm, periodically hexagonal wrinkles were found as shown in Figure 1c,e,f. For films with thickness ≥42 ± 2 nm, chaotic network-like blisters were achieved, similar to previous studies.[15,16] To the best of our knowledge, this is the first observation of long-range periodic buckling on rigid substrates.

2.1. Building Blocks of This Delamination Process and Wrinkle Properties

To study the self-assembly dynamics of these periodic hexagonal pattern, in situ atomic force microscopy (AFM) was used to capture the buckling process at its onset. It was observed that trigeminal shape wrinkles with zigzag backbone (3D AFM image in Figure 1b and dark field optical image in Figure 1d) spontaneously formed and spread in the plane at a constant rate and then converged with adjacent trigeminal wrinkles. Finally, they coalesced into hexagonal wrinkles and propagated as presented in Figure 1c. Unlike previous reports of micrometer scale telephone cord patterns observed for carbon films on rigid substrates, the hexagonal wrinkle produced in this work (Figure 1e) spread uniformly over large area (see Figure 1f) up to centimeter scale and exist stably in air (Figure S6, Supporting Information).[15–17,21,22]

We have tested the formation of wrinkled films on a range of substrates (as shown in **Figure 2**a, Figures S1 and S2, Supporting Information) but only observed the periodic hexagonal wrinkled pattern on *c*-plane sapphire (Figure 1e,f). Besides its low roughness (0.11 nm), the unique lattice structure of *c*-plane sapphire substrate may have a role. *c*-plane sapphire is widely used for the epitaxial growth of material with a hexagonal lattice structure due to its high thermal expansion coefficient.[24,25] One possible model for the growth of graphite on sapphire with reduced lattice mismatch is depicted schematically in Figure 2b. The lattice mismatch between NCG and sapphire is calculated to be ≈2.8% and the small mismatch benefits the epitaxial growth of NCG.[24]

2.2. Evolution of Strain-Relief Features as a Function of Film Thickness

To understand the effect of film thickness on geometry of hexagonal wrinkle, the morphology of wrinkled NCG films of various thicknesses was recorded using noncontact mode

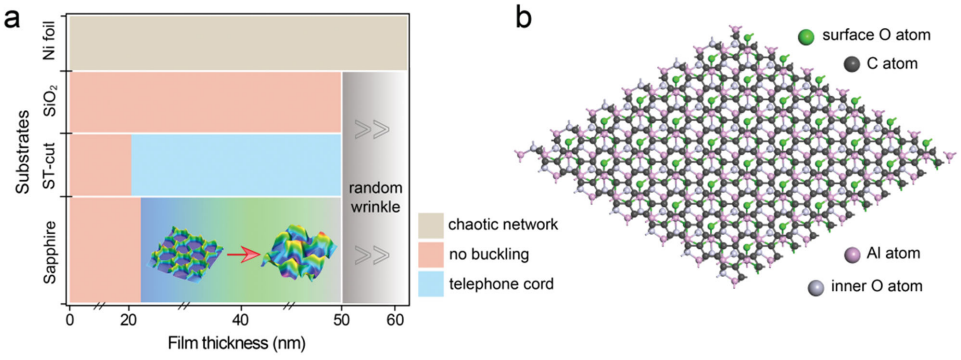

Figure 2. Buckling–delamination patterns of NCG films with varying thickness on different substrates. a) Delamination of NCG thin films of different thickness on single crystal *c*-plane sapphire, single-crystal ST-cut quartz, SiO_2 (quartz substrate and silicon wafer with 300 nm silicon dioxide), and nickel foil, separately. b) Top view of NCG model on sapphire (0001).

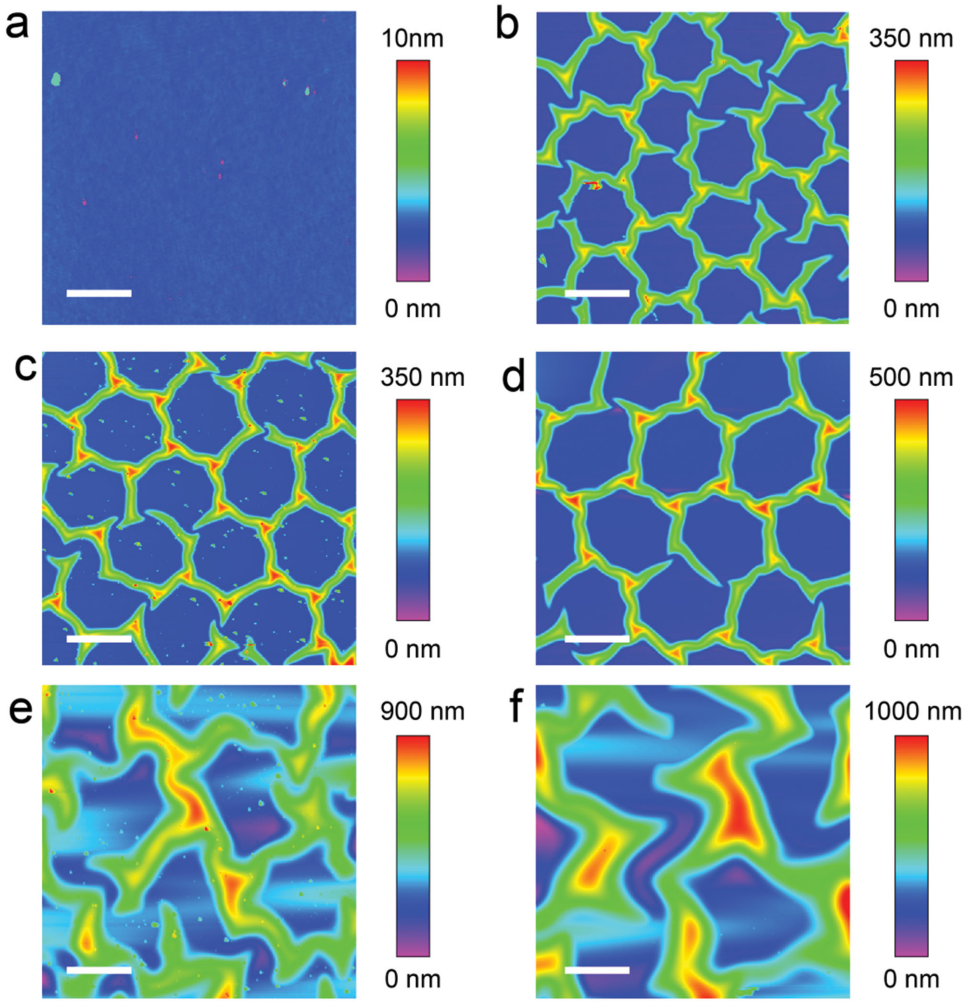

Figure 3. AFM images of NCG film showing thickness-dependent wrinkled pattern. a) Topography of 17 ± 1 nm thick NCG film. Delamination process was not observed for this thickness. b–f) Various delamination patterns of NCG films with different thickness: 24 ± 2.1, 31 ± 2.8, 35 ± 2.7, 42 ± 2.6, and 46 ± 2.9 nm, respectively. More details are summarized in Table 1. All scale bars are 8 μm.

AFM to minimize the deformation caused by AFM tip as shown in **Figure 3**. NCG films with thickness less than 24 nm (see Figure 3a) did not undergo delamination process, while they exhibited disordered pattern once their thickness exceeded 42 nm (Figure 3f). The geometry parameters are summarized in **Table 1**. In the thickness range between 24 and 42 nm, the physical dimensions of hexagonal periodic wrinkles were observed to be dependent on the NCG films thickness. The height, length, and width of the wrinkles increased with the thickness of the NCG film (from Figure 3b–e). The ratio of film thickness and wrinkle width, expressed as $2t/W$, is determined by the critical compressive biaxial stress σ_c and fluctuates within a maximum value (≈0.0295 at ≈31 nm thick NCG films), and then reduces dramatically with further increase in thickness. σ_c is known to be dependent on the Young's modulus and Poisson's ratio of film and substrate.[23] For a fixed system, a decreasing value of $2t/W$ indicates that the film may experience more than one kind of delamination processes. Jagla and Crosby applied a triangular building block model to study the buckling–delamination phenomenon of elastic thin film on rigid substrates.[26,27] In their simulations, the wrinkles bifurcation and branches formation were successfully predicted, but they failed to explain the formation of hexagonal shape wrinkles. This prompted us to select 2D triangles as the repeating unit for fabricating long-range hexagonal-shaped wrinkles as shown in Figure S8 (Supporting Information). The triangular unit was found to fit the hexagonal pattern well, and the dimensions of the triangular units gradually increased for thicker films. The NCG films (35 ± 2.7 nm thick) in Figure S8c (Supporting Information) seem to withstand additional sinusoidal wave deformation besides the hexagonal pattern delamination. It is calculated in the later section that as thickness increases, the hexagonal pattern could not release the internal stress of thick NCG films effectively and hence, other type of deformation occurs to balance the disproportion (in the later section).[28] As the film thickness increased further (>42 nm), sinusoidal wave deformation destroyed the periodic pattern.

Table 1. Physical dimension of the hexagonal wrinkles as a function of film thickness.

Films thickness t [nm]	Height h [nm]	Width W [μm]	Edge length [μm]	Height of intersect [nm]	$\frac{2t}{W}$
17 ± 1.2	N/A	N/A	N/A	N/A	N/A
24 ± 2.1	188 ± 20	2.1 ± 0.18	5.2 ± 1.7	291 ± 21	≈0.0229
31 ± 2.8	215 ± 28	2.1 ± 0.15	6.1 ± 0.9	303 ± 29	≈0.0295
35 ± 2.7	256 ± 31	2.5 ± 0.22	6.6 ± 1.3	380 ± 62	≈0.0280
42 ± 2.6	350 ± 132	5.1 ± 1.6	7.4 ± 2.4	626 ± 203	≈0.0165
46 ± 2.9	430 ± 162	6.3 ± 4.2	9.6 ± 3.3	770 ± 346	≈0.0146

2.3. Theoretical Prediction of Periodic Wrinkle's Geometry Based on Film Thickness

To understand the formation of periodic hexagonal wrinkle and the relation between film thickness and geometry, the normalized elastic energy of the hexagonal wrinkle is calculated.

The underlying substrate is considered as infinitely thick ($t_{sub} \gg t_{film}$), isotropic, and homogeneous. The internal stress of NCG film is isotropic and biaxial prior to delamination.

The von Karman equations representing the NCG thin film in Cartesian coordinates are

$$D_f \nabla^4 w(x,y) + \left(N_{11} w(x,y)_{,11} + N_{22} w(x,y)_{,22} + 2N_{22} w(x,y)_{,12}\right) = -p_s \tag{5}$$

$$\frac{1}{E_f t}\nabla^4 F = w(x,y)_{,12}^2 - w(x,y)_{,11}\, w(x,y)_{,22} \tag{6}$$

Here, $w(x,y)$ is the vertical displacement of the thin film middle surface, $\nabla^4()$ is the biharmonic operator, $D_f = E_f t^3/\left[12\left(1-\nu_f^2\right)\right]$ is the thin film bending stiffness, and t is the thickness of the thin film with E_f and ν_f as its Young's modulus and Poisson's ratio. F is the airy stress function, and p_s is the stress component acting perpendicular to the thin film that is exerted by the sapphire substrate.

The vertical displacement function $w(x,y)$ for the hexagonal wrinkle is represented by

$$w(x,y) = \xi t\left[\cos(kx) + 2\cos\left(\frac{1}{2}kx\right)\cos\left(\frac{\sqrt{3}}{2}ky\right)\right] \tag{7}$$

where ξ is an independent amplitude factor and k scales with the size of the wrinkled pattern. The airy stress function for the hexagonal mode is expressed as[23]

$$\begin{aligned} F = &-\frac{1}{2}(\sigma_0 - \Delta\sigma_1)ty^2 - \frac{1}{2}(\sigma_0 - \Delta\sigma_2)tx^2 \\ &+ \frac{3}{32}E_f t^3 \xi_2^2\left[\cos(kx) - \frac{1}{9}\cos\left(\sqrt{3}ky\right)\right] \\ &- \frac{3}{8}E_f t^3 \xi_1 \xi_2\left[\cos\left(\frac{1}{2}kx\right)\cos\left(\frac{\sqrt{3}}{2}ky\right) + \frac{1}{9}\cos\left(\frac{3}{2}kx\right)\cos\left(\frac{\sqrt{3}}{2}ky\right)\right] \end{aligned} \tag{8}$$

with $\Delta\sigma_1 = \frac{E_f (kt)^2}{4\left(1-\nu_f^2\right)}\left(\xi_1^2 + \frac{1}{8}\xi_2^2\right)$, $\Delta\sigma_2 = \frac{3E_f (kt)^2}{32\left(1-\nu_f^2\right)}\xi_2^2$, and $\xi_2 = 2\xi_1 = \xi$.

For the hexagonal wrinkle, the periodic length is $4\pi/\left(\sqrt{3}k\right)$. In terms of the stress function F and $w(x,y)$, the elastic energy (film bending and stretching) of the carbon thin film after buckling in a periodic cell is[23]

$$\begin{aligned} U = &\int_0^S \frac{D_F}{2}\left[\left(\nabla^2 w\right)^2 + 2(1-\nu_f)\left(w_{,12}^2 - w_{,11}w_{,22}\right)\right]dS \\ &+ \int_0^S \frac{1}{2E_f t}\left[\left(\nabla^2 F\right)^2 + 2(1+\nu_f)\left(F_{,12}^2 - F_{,11}F_{,22}\right)\right]dS \end{aligned} \tag{9}$$

Here, S is the area of the periodic cell. Let σ_0 be the equi-biaxial compressive stress in the unbuckled film, so the elastic energy of the NCG thin film before buckling in a periodic cell is

$$U_0 = \frac{1-\nu_f}{E_f}\sigma_0^2 tS \tag{10}$$

The equi-biaxial compressive stress σ_0 of flat NCG thin film imposed by the substrate before buckling can be approximated by the following expression

$$\sigma_0 = \frac{E_f}{1-\nu_f^2}\left[\frac{2(1+\nu_f)(\Delta l - \Delta l_f)}{l}\right] \tag{11}$$

with $\Delta l = \frac{tE_f\Delta l_f\left(1-\nu_f^2\right)(1+\nu_f) + t_s E_s \Delta l_s\left(1-\nu_s^2\right)(1+\nu_s)}{tE_f\left(1-\nu_f^2\right)(1+\nu_f) + t_s E_s\left(1-\nu_s^2\right)(1+\nu_s)}$, $\Delta l_f = \frac{1}{2}\alpha_f l\Delta T$, and $\Delta l_s = \frac{1}{2}\alpha_s l\Delta T$.

Here E_s, ν_s, and $t_s\left(t_s \gg t\right)$ are Young's modulus, Poisson's ratio, and thickness of the substrate, respectively. α_f and α_s are the thermal expansion coefficients of the carbon film and substrate, respectively. ΔT is the temperature deviation from growth to room temperature, and l is the initial length of the NCG thin film at the growth temperature.

The critical film stress σ_c, characterizing the onset of buckling is[15,18]

$$\sigma_c = \frac{\pi^2 E_f}{12\left(1-\nu_f^2\right)}\left(\frac{2t}{W}\right)^2 \tag{12}$$

where t is the film thickness and W is the full width of the wrinkle.

Using the geometrical parameters derived from AFM and nanoindentation analysis of the hexagonal wrinkles, where E_f = 142 GPa, ν_f = 0.25, $2t/W$ = 0.0295, k = 0.907 μm^{-1}, ξ = −1.8, E_s = 345 GPa, ν_s = 0.28, $\alpha_f = 4 \times 10^{-6}$ K^{-1}, $\alpha_s = 7.5 \times 10^{-6}$ K^{-1}, and ΔT = 700 K,[30] the normalized elastic energies U/U_0 of the NCG thin films are calculated as a function of thickness t and σ_0/σ_c for hexagonal wrinkle, as shown in **Figure 4**a. Using similar procedures, the normalized elastic energies for telephone cord wrinkle are plotted in Figure 4b for comparison (for more calculation details, see Section S9 in the Supporting Information). The low U/U_0 value over the film thickness range of 21.0–52.8 nm suggests that hexagonal wrinkle formation requires a lower buckled elastic energy when overstress σ_0/σ_c = 4 compared to the telephone cord wrinkle. In contrast, the telephone cord

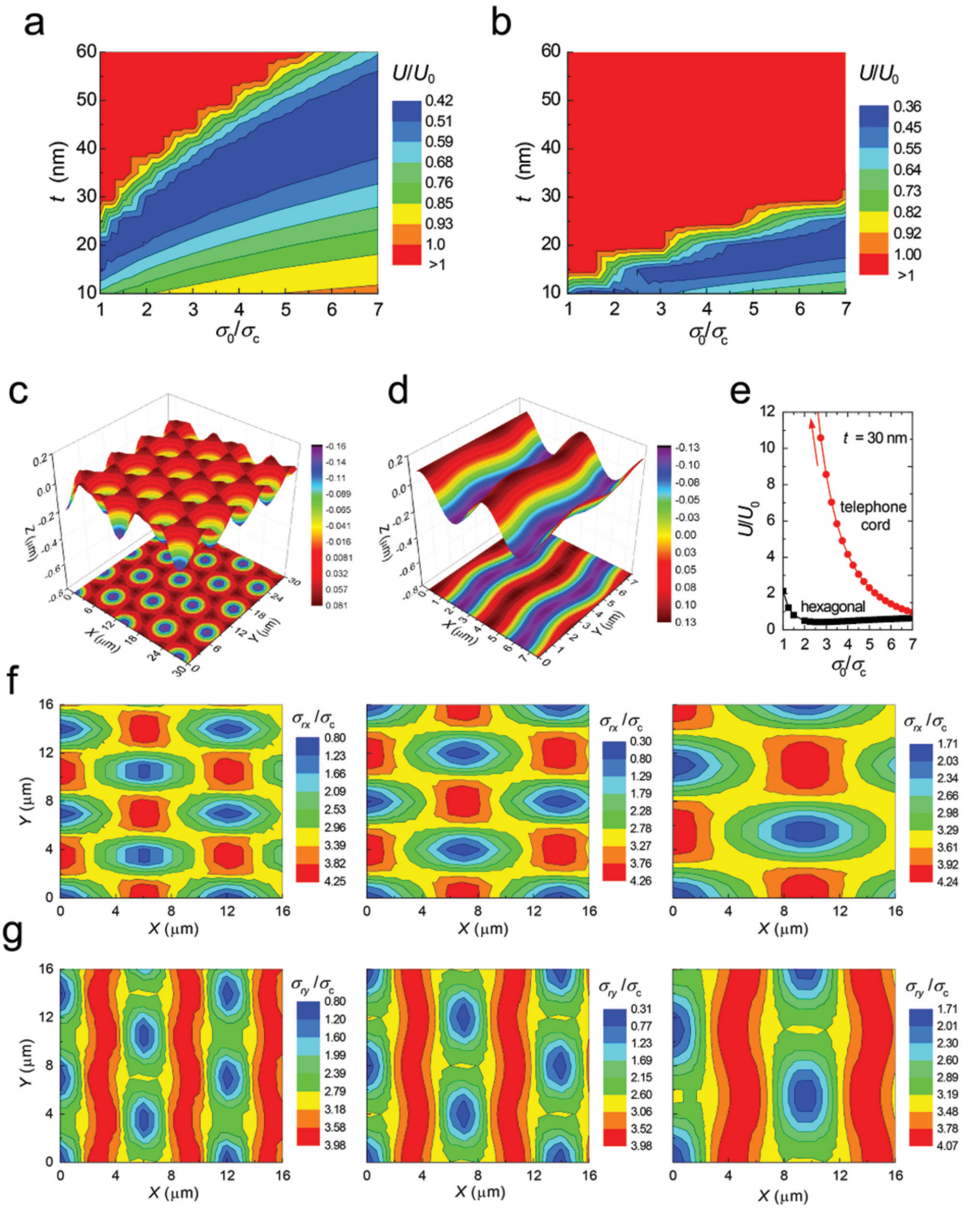

Figure 4. Theoretical calculation of the formation of delaminated hexagonal pattern. a,b) Contour plots of normalized elastic energies U/U_0 of carbon thin films in the hexagonal buckled states and telephone cord buckled states as a function of thickness t and σ_0/σ_c for $\sigma_c = 0.11$ GPa. c) Simulated hexagonal wrinkled pattern of NCG films with a thickness of 30 nm and a periodic length of 8 μm. d) Telephone cord wrinkled pattern of NCG films with a thickness of 30 nm and periodic lengths of 4 and 5 μm in the x and y-directions, respectively. e) Normalized energies U/U_0 of 30 nm thick NCG films in the hexagonal and telephone cord buckled states with the same critical stress ($\sigma_c = 0.11$ GPa). The arrow denotes that the U/U_0 increases sharply when σ_0/σ_c decreases. f,g) The remaining stresses in x and y-directions of the hexagonal wrinkled carbon film with thickness of 25, 30, and 35 nm (from left to right).

wrinkle on NCG film will form at thickness <21.0 nm or at a larger compressive stress σ_0 regime. When $U/U_0 \geq 1$, no hexagonal wrinkled pattern can form.

In the NCG/sapphire system, for $\sigma_0/\sigma_c = 4$, it can be seen from Figure 4a,b that the normalized elastic energies U/U_0 reach a minima at a thickness of 15 nm for the telephone cord wrinkle while the energy minima is attained at 28 nm for hexagonal wrinkle. This result indicates that the hexagonal wrinkle is preferred in thicker film compared to the telephone cord wrinkle. The variation in the normalized elastic energy as a function of overstress σ_0/σ_c for these two different patterns is also investigated. Figure 4e shows the variations of U/U_0 for a 30 nm thick NCG film in the hexagonal (Figure 4c) and telephone cord (Figure 4d) wrinkles. For σ_0/σ_c values of 1–7, the elastic energy of the telephone cord wrinkle is larger than that of the hexagonal wrinkle and decreases sharply when overstress increases. This demonstrates that a higher overstress is needed to form the telephone cord wrinkle for 30 nm thick NCG film.

The remaining stress in the wrinkled NCG film after buckling is calculated by

$$\sigma_{rx} = \left(\frac{\partial^2 F}{\partial y^2}\right)/t, \sigma_{ry} = \left(\frac{\partial^2 F}{\partial x^2}\right)/t \quad (13)$$

For the hexagonal wrinkle, Figure 4f,g shows the remaining stresses along the x and y-directions of NCG film with different thicknesses, which may play important role in the stem cell differentiation (more details are discussed in the stem cell section). The average remaining stress σ_{rx} and σ_{ry} are 0.317 and 0.321 GPa for 25 nm thick film, 0.245 and 0.287 GPa for 30 nm thick film, and 0.358 and 0.364 GPa for the 35 nm thick film, respectively. Higher remaining stress in the 35 nm thick film will certainly undergo other type of deformation to further release the internal stress, for example, undergoing sinusoidal wave deformation, as discussed in the previous section.

2.4. Shock Absorbability of NCG Films

In order to estimate the pressure buffering ability of out-of-plane wrinkles, real-time peak force QNM (quantitative nanomechanical property mapping, Bruker Dimension FastScan AFM) technique was performed to analyze the mechanical properties of these NCG films.[30] First, the topographies under different loading forces in the same area were captured (loading force: 500 nN for **Figure 5**a; 1500 nN for Figure 5b; and full data in Figure S9 in the Supporting Information). The responses to loading force of one representative wrinkle were summarized

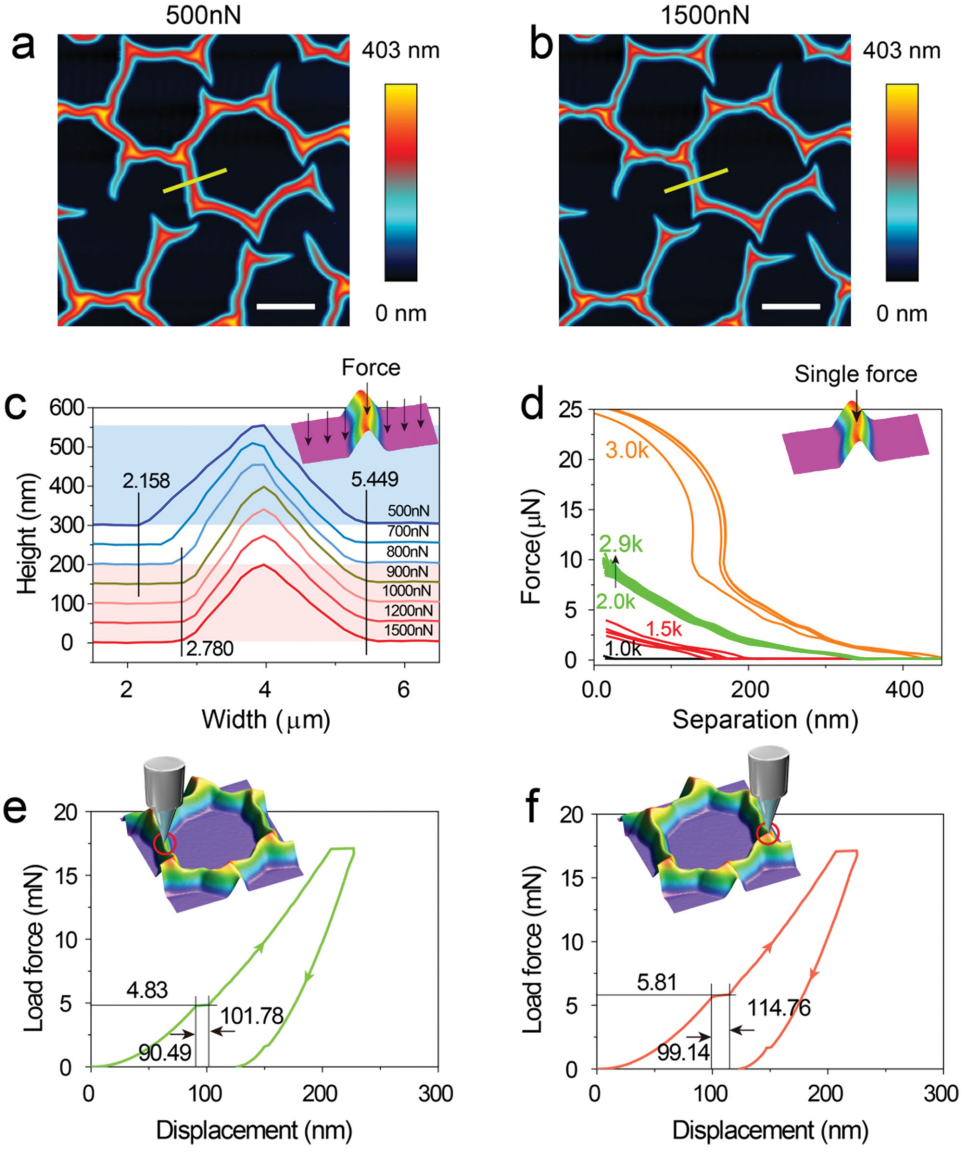

Figure 5. Mechanical properties of NCG films. a,b) AFM topographies of wrinkled NCG films under various loading forces, a) 500 and b) 1500 nN, respectively . Scale bars are 8 μm. c) Wrinkle geometry deformation under varying loading forces applied on AFM tip. d) Wrinkle vertebra's resistivity to different loading forces. e,f) Nanoindentation load–displacement responses from wrinkled vertebra and intersect region.

in Figure 5c. Under loading, the height of the wrinkles gradually decreased to ≈195 nm (dark red line, 1500 nN) from ≈255 nm (dark blue line, 500 nN). After the loading force was released, all the wrinkles were found to be restored to the initial height. The elasticity of the wrinkled pattern suggests that it can act as excellent shock absorber in flexible, transparent, and conductive coatings. To further investigate its elastic section modulus, the deformation of the spine part of the wrinkled pattern (inserted AFM image in Figure 5d) was examined under varying loading forces. In this measurement, the height of this wrinkle was first determined by tapping AFM. After that, the AFM tip was pushed onto the sample to apply a loading force (varying from 1000 to 3000 nN) and then lifted away from the sample. During this period, the cantilever forces were recorded as a function of the separation distance of AFM cantilever tip and sample in the *z*-direction. From the force versus separation plot in Figure 5d, the wrinkles collapsed completely once the loading force was ≥2000 nN (during this process, no obvious indentation into the samples was observed), which translate to external threshold pressure in the magnitude of ≈8.0 GPa. (Young's modulus of graphene is ≈1 TPa but graphene has no elastic section modulus due to its 2D structure; theoretical and experimental effective elastic radial modulus of single-walled carbon nanotube (SWCNTs) with tube diameter of 2.38 nm is ≈5.5 GPa.)[31,32]

To reconfirm the mechanical results from QNM AFM, nanoindentation was employed.[33] In the flat region, no in-plane slippage-induced crack was observed during loading (its typical loading–unloading cycle is shown in Figure S10a in the Supporting Information). To minimize the contribution of underlying sapphire substrate, calculation of the Young's modulus and hardness was based on nanoindentation up to 10% of the total NCG film thickness (displacement ≤3–4 nm) (Figure S10, Supporting Information). The fitted hardness (H) and Young's modulus (E) of NCG films were 7.27 ±3.8 GPa and 142 ± 80 GPa, respectively, which are slightly higher than that of glassy carbon (H ≈2–3 GPa, E ≈30 GPa, while for diamond-like carbon, the values are H ≈12–30 GPa and E ≈62–213 GPa).[34,35] Due to the existence of intersected node, the elastic section modulus might be underestimated. To qualitatively estimate the pressure resistance of the wrinkled patterns, we compared their force–displacement curves (Figure 5e,f) from the spine and node region with the same input parameters. The node's curve showed relatively late and long pop-in event and slightly smaller displacement, indicating that it is stiffer than the spine regions.

2.5. High-Fidelity Dry Transfer of Wrinkled NCG Film onto Arbitrary Substrates

The weak interaction between buckled NCG films and sapphire substrate enables a facile etch-free dry transfer of the delaminated/buckled film onto arbitrary substrates and the recycle of sapphire substrate for further growth.[5,6,8–13]

As shown in **Figure 6**, after completion of the CVD growth and buckling process, the wrinkled NCG film was loaded into thermal evaporator for gold deposition (50 nm). The purpose of this metal deposition was to increase the hardness of wrinkled films and to avoid the direct conglutination of adhesive and NCG films. UV-curable optical adhesive or thermal adhesive was spun onto intermediate glass, PDMS, or PET film. After this, the adhesive/intermediate substrate was placed carefully onto gold/NCG films to avoid any bubble. After solidification, NCG/gold bilayer structure could be easily peeled off (Figure 6d,e) from sapphire substrates, as shown in Figure 6h. By repeating the above steps (Figure 6c,e), the periodically wrinkled NCG films could be efficiently transferred onto target substrate while maintaining its shape and periodicity (Figure S7, Supporting Information). The absence of gold residue after the transfer process was confirmed by XPS, which is indicative of a clean transfer process. The ability to transfer the wrinkled film onto any arbitrary substrate opens up possibilities to use these films in optical or electronic applications. For example we have applied these wrinkled films in electromagnetic interference shielding and found that they showed improved shielding compared to the flat carbon films of equivalent thickness (see supporting information Figure S15).

2.6. Mesenchymal Stem Cell Differentiation into Osteogenic Lineage

In recent years, carbon-based nanomaterials, such as carbon nanotubes and graphene, have been demonstrated to promote stem cell growth and differentiation.[36,37] Substrate topography has been demonstrated to be one of the direct and/or indirect mediators of stem cell lineage regulation. The nanotopographical cues originating from synthetic nanostructures are capable of directly stimulating the differential gene expressions of hMSCs.[38] As such, we hypothesized that the highly corrugated NCG films here may provide biophysicochemical cues to the stem cells, resulting in the upregulation of certain gene expressions corresponding to specific lineage differentiation. To verify this, we seeded hMSCs on various fibronectin-coated wrinkled NCG substrates and probed how these substrates would influence differentiation. Fibronectin is an important glycoprotein typically used for facilitating cell adhesion and is involved in cell migration and differentiation.[39] The hMSCs were cultured on these substrates in the presence of growth medium and then stained with specific protein biomarkers on day 7 and day 14 to identify their lineage specifications: Runx2 and Osteopontin (OPN) for early and late osteogenic (bone), respectively, PPARγ2 for adipogenic (fat), and Desmin for myogenic (muscle) differentiations (**Figure 7**, Figures S12 and S13, Supporting Information). To confirm the presence of the cells, the nuclei of all the hMSCs were stained with 4′,6-diamidino-2-phenylindole (DAPI).

The immunofluorescence images of the hMSCs cultured on six different carbon substrates showed selective differentiation toward the osteogenic lineage, in particular, for hMSCs seeded on substrates T_2, T_3, and T_4, with film thicknesses ranging from 25 to 35 nm, respectively (Figure 7a) (T_2–T_5 represent hexagonally wrinkled NCG films with various thicknesses). We observed that substrate T_2 induced the highest osteogenic differentiation based on the highest expressions of Runx2 on day 7 (Figure 7b) and OPN on day 14 (Figure 7c), followed by substrates T_3 and T_4. Generally, Runx2 is a transcription factor

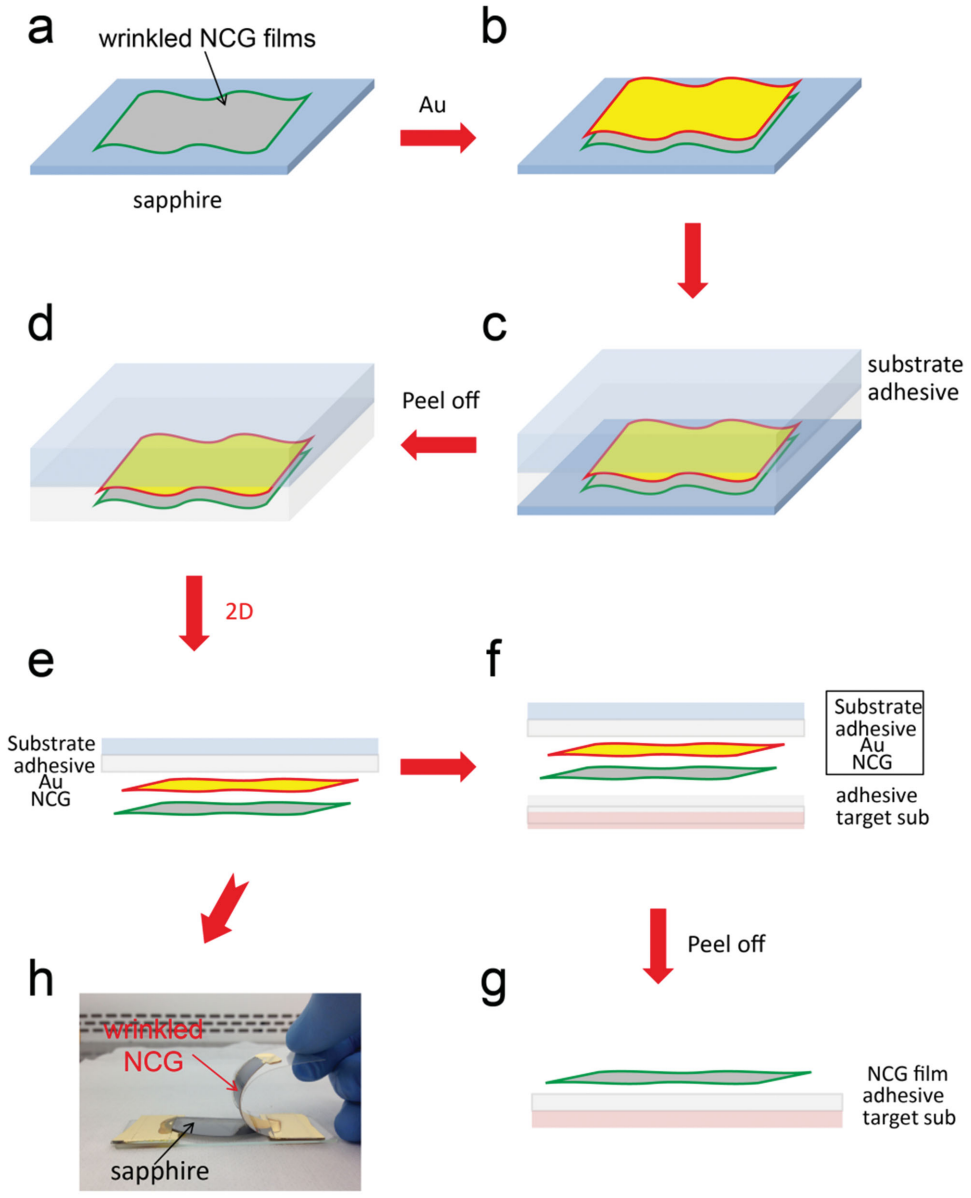

Figure 6. Transfer process of wrinkled NCG film onto arbitrary substrate. a) Wrinkled NCG film on sapphire. b) Thermal evaporation of 50 nm gold onto NCG/sapphire. c) Intermediate substrate (PET or glass slide) is placed onto NCG/sapphire substrate with small amount of optical adhesive (Norland optical adhesive 61) or thermal adhesive (EPO-TEK 353ND). d,e) Upon adhesive solidification and peeling off, NCG film is left on the intermediate substrate. f,g) Repeating step (c) and (d), NCG film is transferred onto target substrates. h) Optical images of the peel off process of wrinkled NCG films from sapphire substrates.

which activates the osteoblast specific genes while OPN marks the activity of osteoblasts. The production of these matrix proteins indicates the maturation of the osteoblast cells and the subsequent mineralization. In contrast, hMSCs which were seeded on flat, T_5, and TC (telephone cord wrinkles, AFM image in Figure S11 in the Supporting Information) substrates did not exhibit any tendency of differentiating into osteogenic lineage. Furthermore, we did not observe significant expressions of PPARγ2 and Desmin in these stem cells. This suggests that the hMSCs cultured on all carbon substrates did not differentiate into fat and muscle cells (Figures S12 and S13, Supporting Information).

It is important to note that hMSCs were maintained in the growth medium without the presence of any chemical inducer. Interestingly, hMSCs on hexagonal wrinkled substrates T_2, T_3, and T_4 differentiated into bone cells in the absence of osteogenic agents and growth factors necessary for osteogenic differentiation, such as dexamethasone and BMP-2. We believe that the observed phenomenon was not mediated by the chemical interactions between cells and substrates because all carbon substrates possess inherently similar chemical properties. The enhancement was also not likely to be controlled by substrate elasticity since the stiffness of all carbon films was in the range of a few GPa. Instead, evidences suggest that the enhanced

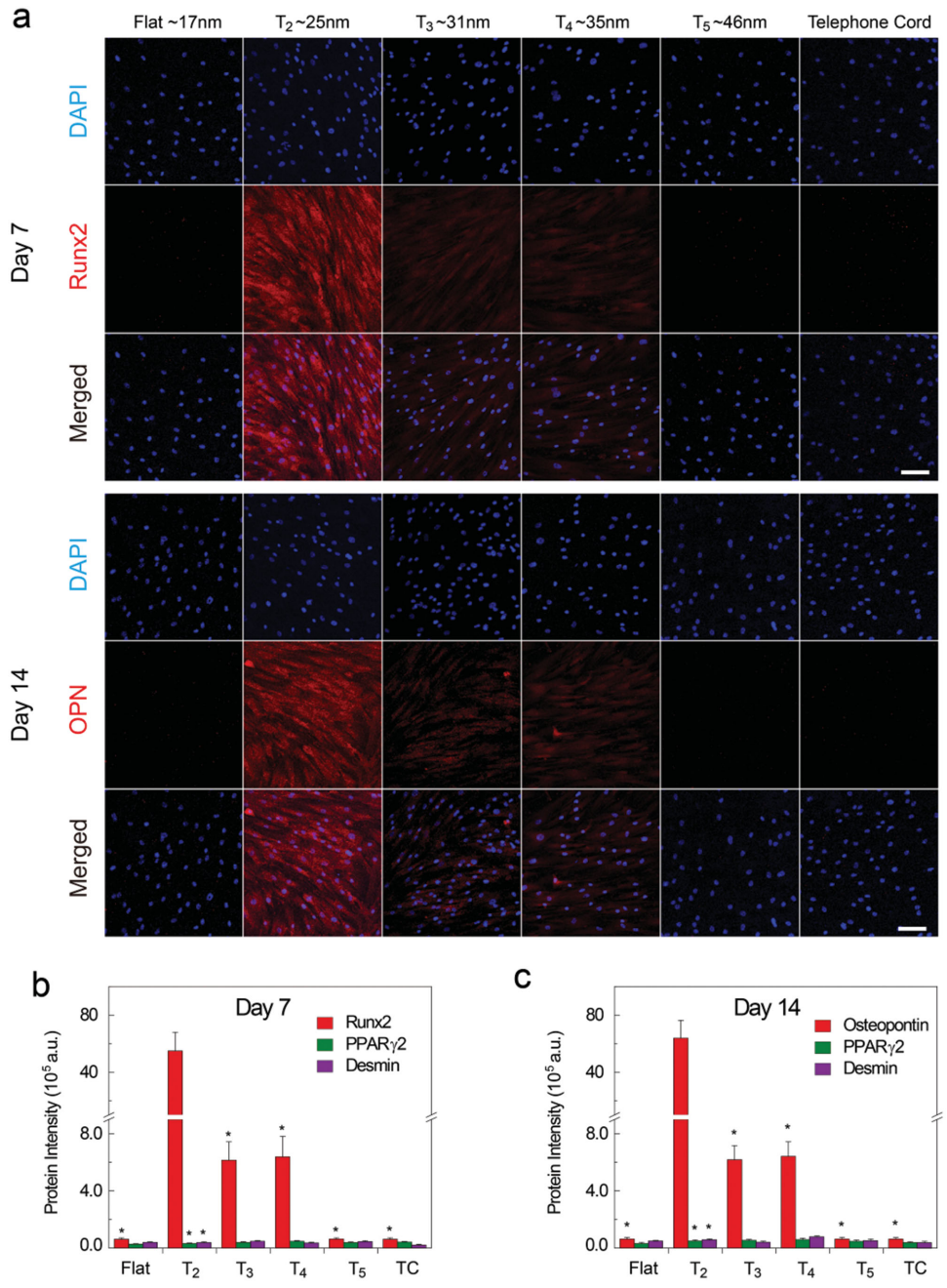

Figure 7. Mesenchymal stem cell differentiation on various NCG substrates. a) Representative images showing the osteogenic differentiation of the human mesenchymal stem cells (hMSCs) taken on day 7 and day 14. "Flat" indicates flat NCG film. T_2–T_5 represent the NCG films full of hexagonal wrinkles with various thicknesses. Telephone cord (TC) is the widely observed telephone cord wrinkled NCG films from ST-cut substrates and its NCG thickness is ≈30 nm. All scale bars represent 20 μm. b,c) Corresponding protein intensity of the various biomarkers used to detect the differentiation of hMSCs on the different NCG films: Runx2 and OPN (Osteopontin) for osteogenic (bone), PPARγ2 for adipogenic (fat), and Desmin for myogenic (muscle) differentiations. The * represents statistically significant differences for *p*-values < 0.01 based on the Student's *t*-test. All comparisons were made with respect to the b) Runx2 and c) OPN markers of wrinkled substrate T_2 (thickness ≈25 nm) on day 7 and day 14, respectively.

osteogenic differentiation of hMSCs on substrates T_2, T_3, and T_4 may originate from the nanotopographical features in appropriately wrinkled films, these support a smaller interprotein aggregate spacing and a higher local concentration of adhesion proteins. In this regard, we note that the hexagonal wrinkles have a longer range periodicity compared to the telephone cord wrinkles in the NCG films, thus giving rise to a higher density of nanotopographical features per unit area. Numerous studies have reported the enhancement of stem cell differentiation into specific cell lineages through surface topography–induced physical stresses.[37–48] A high surface adsorption of fibronectin has also been directly correlated to an improved

osteoblast adhesion.[42,43] Interestingly, recent work showed that a higher periodicity[43] and a lower nanoscale height[49] of surface topographical features play key roles in regulating the stem cell fate. Therefore, with the highest percentage of wrinkled regions per unit area (percentage of wrinkled and strained regions, 34.8% for T_2, 29.3% for T_3, and 26.4% for T_4) as well as enjoying a much longer range of the wrinkled features and lower nanoscale height, substrate T_2 is expected to enhance the adsorption of fibronectin. Increasing the local concentration of adhesion molecules and proteins results in a denser packing of protein mules. Highly wrinkled films may influence the signaling pathways activating the osteogenesis-related genes, resulting in osteogenic differentiation.

3. Conclusion

Large-area hexagonal-shaped wrinkles were produced via the buckling–delamination of CVD NCG on single crystal sapphire substrates (0001). The generation of hexagonal-patterned wrinkles is correlated to its lower elastic energy in comparison with telephone cord pattern. Our elastic energy calculations predicted correctly the film thickness, wrinkle heights, and stress release efficiency in the hexagonal pattern. It is found that under the same stress condition ($\sigma_0/\sigma_c = 4.2$) the elastic energy and average remaining stress of 30 nm thick hexagonal wrinkled film are the lowest. We have also developed a high-fidelity transfer method for these wrinkled NCG films onto arbitrary substrates, thus opening the possibility to deploy these corrugated films in various applications. The surface wrinkles impart a high elastic section modulus (up to 8 GPa) on the NCG film, suggesting its application as a shock absorber or pressure sensor. The wrinkled films provide mechanical–topographical cues for the selective osteogenic differentiation of human mesenchymal stem cells in the absence of osteogenic inducer. This work successfully demonstrated the generation and application of highly periodic wrinkles on CVD growth films for various technological applications.

4. Experimental Section

Chemical Vapor Deposition of Thin Flat NCG Films and Its Buckling: Sapphire wafers (Al_2O_3, *c*-plane (0001)) were precleaned in oxygen atmosphere at 900 °C for 30 min to remove any contaminants in tube furnace. After cooling to room temperature, the system was purged with argon gas for 15 min and heated to 1000 °C within 30 min and held at that temperature for 5 min. Toluene solution (selected as the carbon source, and stabilized at 60 °C in circulator bath) was introduced by bubbling 8 sccm argon gas to start the growth. The growth was stopped at different times to control thickness and then cooled down to room temperature. Depending on the thickness of NCG films, the wrinkle appeared at different time. For thick carbon films (≥50 nm), the buckling occurred at the moment that the samples were taken out the tube. While for thinner NCG films, it happened overnight.

Mesenchymal Stem Cell Culture: hMSCs (Lonza Inc.) were maintained in the hMSC growth medium (Lonza Inc.) supplemented with 1% penicillin/streptomycin (Invitrogen). Fibronectin of 50 μg mL^{-1} was coated on the various carbon substrates and ≈1000 cells cm^{-2} were then seeded onto the fibronectin-coated substrates. DAPI was used to stain the nuclei of all stems cells while Runx2 and Osteopontin were used as the early and late osteogenic (bone) differentiation markers, respectively.

Supporting Information

Supporting Information is available from the Wiley Online Library or from the author.

Acknowledgements

The authors appreciate M. Yang for helpful discussion and T. W. Goh (Glen) from IMRE for performing the nanoindentation test.

Received: May 15, 2015
Revised: June 19, 2015
Published online: August 3, 2015

[1] S. J. Kang, C. Kocabas, T. Ozel, M. Shim, N. Pimparkar, M. A. Alam, S. V. Rotkin, J. A. Rogers, *Nat. Nanotechnol.* **2007**, *2*, 230.
[2] K. S. Kim, Y. Zhao, H. Jang, S. Y. Lee, J. M. Kim, K. S. Kim, J.-H. Ahn, P. Kim, J.-Y. Choi, B. H. Hong, *Nature* **2009**, *457*, 706.
[3] Y. Zhou, K. P. Loh, *Adv. Mater.* **2010**, *22*, 3615.
[4] W. Bao, F. Miao, Z. Chen, Z. Hang, W. Jang, C. Dames, C. N. Lau, *Nat. Nanotechnol.* **2009**, *4*, 562.
[5] M. W. Moon, S. Chung, K. R. Lee, K. H. Oh, H. A. Stone, J. W. Hutchinson, *Int. J. Mater. Res.* **2007**, *98*, 1203.
[6] J. Yin, J. L. Yague, D. Eggenspieler, K. K. Gleason, M. C. Boyce, *Adv. Mater.* **2012**, *24*, 5441.
[7] B. H. Kim, Y. Choi, J. Y. Kim, H. Shin, S. Kim, S. W. Son, S. O. Kim, P. Kim, *Adv. Mater.* **2014**, *26*, 4665.
[8] M. W. Moon, S. H. Lee, J. Y. Sun, K. H. Oh, A. Vaziri, J. W. Hutchinson, *Proc. Natl. Acad. Sci. USA* **2007**, *104*, 1130.
[9] C. F. Guo, V. Nayyar, Z. Zhang, Y. Chen, J. Miao, R. Huang, Q. Liu, *Adv. Mater.* **2012**, *24*, 3010.
[10] H.-S. Kim, A. J. Crosby, *Adv. Mater.* **2011**, *23*, 4188.
[11] U. N. Maiti, J. Lim, K. E. Lee, W. J. Lee, S. O. Kim, *Adv. Mater.* **2014**, *26*, 615.
[12] J. Shim, J. M. Yun, T. Yun, P. Kim, K. E. Lee, W. J. Lee, R. Ryoo, D. J. Pine, G. R. Yi, S. O. Kim, *Nano Lett.* **2014**, *14*, 1388.
[13] N. Bowden, S. Brittain, A. G. Evans, J. W. Hutchinson, G. M. Whitesides, *Nature* **1998**, *393*, 146.
[14] A. Schweikart, N. Pazos-Pérez, R. A. Alvarez-Puebla, A. Fery, *Soft Matter* **2011**, *7*, 4093.
[15] N. Matuda, S. Baba, A. Kinbara, *Thin Solid Films* **1981**, *81*, 301.
[16] S. B. Iyer, K. S. Harshavardhan, V. Kumar, *Thin Solid Films* **1995**, *256*, 94.
[17] G. Gille, B. Rau, *Thin Solid Films* **1984**, *120*, 109.
[18] M. W. Moon, K. R. Lee, K. H. Oh, J. W. Hutchinson, *Acta Mater.* **2004**, *52*, 3151.
[19] M. W. Moon, H. M. Jensen, J. W. Hutchinson, K. H. Oh, A. G. Evans, *J. Mech. Phys. Solids* **2002**, *50*, 2355.
[20] J. W. Hutchinson, Z. Suo, *Adv. Appl. Mech.* **1991**, *29*, 63.
[21] S. Peponas, M. Guedda, M. Benlahsen, *Solid State Commun.* **2008**, *146*, 78.
[22] Y. J. Zhang, S. J. Yu, H. Zhou, M. G. Chen, Z. W. Jiao, *Surf. Rev. Lett.* **2012**, *19*, 1250022.
[23] S. Cai, D. Breid, A. J. Crosby, Z. Suo, J. W. Hutchinson, *J. Mech. Phys. Solids* **2011**, *59*, 1094.
[24] J. Hwang, M. Kim, D. Campbell, H. A. Alsalman, J. Y. Kwak, S. Shivaraman, A. R. Woll, A. K. Singh, R. G. Hennig, S. Gorantla, M. H. Rümmeli, M. G. Spencer, *ACS Nano* **2013**, *7*, 385.
[25] S. K. Jerng, D. S. Yu, Y. S. Kim, J. Ryou, S. Hong, C. Kim, S. Yoon, D. K. Efetov, P. Kim, S. H. Chun, *J. Phys. Chem. C* **2011**, *115*, 4491.
[26] E. A. Jagla, *Phys. Rev. B* **2007**, *75*, 085405.
[27] K. M. Crosby, R. M. Bradley, *Phys. Rev. E* **1999**, *59*, R2542.
[28] M. Y. Yang, J. S. Huang, *Compos. Struct.* **2005**, *71*, 229.

[29] W. M. Yim, R. J. Paff, *J. Appl. Phys.* **1974**, *45*, 1456.
[30] M. E. Dokukin, I. Sokolov, *Langmuir* **2012**, *28*, 16060.
[31] M. Zheng, X. Chen, I. T. Bae, C. Ke, C. Park, M. W. Smith, K. Jordan, *Small* **2012**, *8*, 116.
[32] M. Zheng, C. Ke, I.-T. Bae, C. Park, M. W. Smith, K. Jordan, *Nanotechnology* **2012**, *23*, 095703.
[33] C. Lee, X. Wei, J. W. Kysar, J. Hone, *Science* **2008**, *321*, 385.
[34] J. Robertson, *Surf. Coat. Technol.* **1992**, *50*, 185.
[35] N. Savvides, T. J. Bell, *Thin Solid Films* **1993**, *228*, 289.
[36] W. C. Lee, C. H. Y. X. Lim, H. Shi, L. A. L. Tang, Y. Wang, C. T. Lim, K. P. Loh, *ACS Nano* **2011**, *5*, 7334.
[37] X.M. Li, H.F. Liu, X. F. Niu, B. Yu, Y. B. Fan, Q. L. Feng, F. Z. Cui, F. Watari, *Biomaterials* **2012**, *33*, 4818.
[38] B. K. Teo, S. T. Wong, C. K. Lim, T. Y. Kung, C. H. Yap, Y. Ramagopal, L. H. Romer, E. K. Yim, *ACS Nano* **2013**, *7*, 4785.
[39] N. Matsui, K. Nozaki, K. Ishihara, K. Yamashita, A. Nagai, *Mater. Sci. Eng. C* **2015**, *48*, 378.
[40] G. H. Altman, R. L. Horan, I. Martin, J. Farhadi, P. R. Stark, V. Volloch, J. C. Richmond, G. Vunjak-Novakovic, D. L. Kaplan, *FASEB J.* **2002**, *16*, 270.
[41] J. O. Gallagher, K. F. McGhee, C. D. Wilkinson, M. O. Riehle, *IEEE Trans. Nanobiosci.* **2002**, *1*, 24.
[42] S. Oh, K. S. Brammer, Y. S. J. Li, D. Teng, A. J. Engler, S. Chien, S. Jin, *Proc. Natl. Acad. Sci. USA* **2009**, *106*, 2130.
[43] R. K. Das, O. F. Zouani, C. Labrugère, R. Oda, M.-C. Durrieu, *ACS Nano* **2013**, *7*, 3351.
[44] M. J. Dalby, N. Gadegaard, R. Tare, A. Andar, M. O. Riehle, P. Herzyk, C. D. W. Wilkinson, R. O. C. Oreffo, *Nat. Mater.* **2007**, *6*, 997.
[45] D. Khang, M. Sato, R. L. Price, A. E. Ribbe, T. J. Webster, *Int. J. Nanomed.* **2006**, *1*, 65.
[46] S. R. Sousa, M. Lamghari, P. Sampaio, P. Moradas-Ferreira, M. A. Barbosa, *J. Biomed. Mater. Res. A* **2008**, *84*, 281.
[47] P. E. Scopelliti, A. Borgonovo, M. Indrieri, L. Giorgetti, G. Bongiorno, R. Carbone, A. Podesta, P. Milani, *PLoS One* **2010**, *5*, e11862.
[48] S. Oh, K. S. Brammer, Y. J. Li, D. Teng, A. J. Engler, S. Chien, S. Jin, *Proc. Natl. Acad. Sci. USA* **2009**, *106*, 2130.
[49] T. Sjöström, M. J. Dalby, A. Hart, R. Tare, R. O. Oreffo, B. Su, *Acta Biomater.* **2009**, *5*, 1433.